



1 **Airborne bacteria viability and air quality: a protocol to quantitatively investigate the**
2 **possible correlation by an atmospheric simulation chamber**

3
4 *Virginia Vernocchi*¹, *Elena Abd El*^{1,2}, *Marco Brunoldi*^{1,2}, *Silvia Giulia Danelli*¹, *Elena Gatta*²,
5 *Tommaso Isolabella*^{1,2}, *Federico Mazzei*^{1,2*}, *Franco Parodi*¹, *Paolo Prati*^{1,2}, *Dario Massabò*^{1,2}

6
7 ¹ INFN, Sezione di Genova, via Dodecaneso 33, 16146 Genova, Italy

8 ² Dipartimento di Fisica, Università di Genova, via Dodecaneso 33, 16146 Genova, Italy

9
10 *Keywords:* measure technique for bioaerosol, airborne bacteria, Atmospheric Simulation
11 Chambers.

12 * *Corresponding author:* Federico Mazzei; federico.mazzei@ge.infn.it

13

14 **Abstracts**

15 Biological Particulate Matter or bioaerosol are a subset of atmospheric aerosol. They influence
16 climate, air quality and health via several mechanisms which often are poorly understood. In
17 particular, the quantitative study of possible relationship between bioaerosol viability and air
18 quality or meteorological conditions is an open and relevant issue. The difficulty of retrieving such
19 possible correlations by analyses of data collected during in-field campaigns, can benefit of
20 targeted experiments conducted in well controlled conditions inside Atmospheric Simulation
21 Chambers, ASCs. ChAMBRe (Chamber for Aerosol Modelling and Bio-aerosol Research) is an
22 ASC in Genoa (Italy) designed and built to perform experimental research on bioaerosol. In this
23 article we focus on bacteria viability. A multi-step protocol was developed and thoroughly tested:
24 cultivation of a suitable bacteria population, nebulization and injection in the chamber of viable
25 cells, exposure and monitoring of the viability variation inside ChAMBRe, hold at selected
26 conditions, and finally incubation and counting of the concentration of viable bacteria. The whole
27 procedure showed a reproducibility at the 20% level when ChAMBRe is kept in a reference
28 “baseline” condition. This figure quantifies the protocol sensitivity as well to changes in viability
29 when bacteria are exposed in other (e.g., polluted) conditions. First results showing a viability
30 reduction observed exposing the *E. coli* strain to NO_x concentrations and solar irradiation are



31 presented and discussed. Present results pave the way to systematic studies aimed at the definition
32 of dose-effect relationship for several bacteria strain at atmospheric pollutants.

33

34 **1. Introduction**

35 This article focusses on *bioaerosol*, the aerosol of biological origin. The major types of bioaerosols
36 are primary and secondary biological aerosols and biogenic aerosols.

37 Primary biological aerosols (PBAs) refer to bioaerosols that are directly released into the
38 atmosphere from biological sources, such as plants, animals, or microorganisms; these aerosols
39 can be composed of various biological materials, including bacteria, viruses, fungi, pollen, spores,
40 algae, or other organic particles (Ariya and Amyot, 2004; Fröhlich-Nowoisky et al., 2016).

41 Secondary biological aerosols (SBA) are the result of environmental processes or human activities
42 that modify or transform primary biological aerosols. Unlike primary biological aerosols, SBA are
43 not directly released from biological sources but are generated through secondary processes, like
44 oxidation, condensation, etc., involving biological materials. Examples of these SBA are dimethyl
45 sulfide and other volatile organic carbons such as methane (Morris et al., 2014).

46 The PBAs can vary in size depending on the specific biological material being aerosolized; they
47 can range from several nanometers (e.g., viruses, cell fragments) to a few hundred micrometers in
48 aerodynamic diameter (e.g., pollen, plant debris) (Pöschl, 2005). Larger particles of biological
49 material, such as large pollen grains or larger fragments of plants or insects, can be lifted into the
50 air; however, due to their relatively high settling velocities, they tend to rapidly settle or deposit
51 onto surfaces rather than remain suspended in the air for extended periods. As a result, these larger
52 particles are typically not considered atmospheric aerosol particles (Després et al., 2012).

53 Among all the different bioaerosol microorganisms, bacteria are considered to play a significant
54 role in the composition and dynamics of bioaerosols (Bowers et al., 2011). They are ubiquitous in
55 the atmosphere, and their presence and abundance can vary depending on factors such as location,
56 season, and local environmental conditions: usually, over the land, the concentration in atmosphere
57 is greater than 10^4 cells m^{-3} (Bauer et al., 2002) while, over the sea, it tends to be lower, usually by
58 a factor of about 100 to 1,000. This lower concentration is primarily attributed to the relatively
59 cleaner marine environment and the reduced availability of bacterial sources compared to
60 terrestrial environments (Prospero et al., 2005; Griffin et al., 2006;).



61 Bacteria have a relatively long atmospheric residence time, of the order of several days or more,
62 compared to larger particles and can be transported over long distances, up to thousands of km
63 (Després et al., 2012). Airborne bacteria may be suspended as individual cells or attached to other
64 particles, such as soil or leaf fragments, or found as agglomerates of many bacterial cells
65 (Lighthart, 2006). For this reason, whereas individual bacteria are typically on the order of $\sim 1 \mu\text{m}$
66 or less in size, the median aerodynamic diameter of particles containing culturable bacteria at
67 several continental sites has been reported to be $\sim 2 - 4 \mu\text{m}$ (Shaffer and Lighthart, 1997; Tong and
68 Lighthart, 1999; Wang et al., 2007).

69 Even if up to now several works have contributed to the identification of bacterial diversity in the
70 atmosphere (Amato et al., 2007; Burrows et al., 2009; Després et al., 2012, Romano et al., 2019),
71 it remains difficult to establish a clear picture of the actual abundance and composition of bacteria
72 in the air.

73 Numerous studies have suggested that the presence of bacteria in the atmosphere can have
74 significant implications for cloud formation, atmospheric chemistry, microbial biogeography, and
75 climate. As a matter of fact, bacteria can serve as ice nucleating particles and cloud condensation
76 nuclei, influencing the precipitation processes, affecting cloud lifetime, optical properties, and
77 climate patterns (Bauer et al., 2003; Morris et al., 2004; Sun and Ariya, 2006; Möhler et al., 2007).
78 Since bacteria have also been shown to metabolize within cloud droplets, some authors have
79 proposed an impact on the chemistry of cloud droplets and air (Ariya et al., 2002; Ariya and
80 Amyot, 2004; Amato et al., 2005, 2006, 2007; Deguillaume et al., 2008). Finally, the presence of
81 bacteria in the atmosphere can influence microbial biogeography (Martiny et al., 2006) by
82 facilitating long-distance dispersal and the establishment of microbial populations in new
83 environments.

84 Bacteria can enter the atmosphere as aerosol particles from various surfaces, including soil, water,
85 and plant surfaces (Burrows et al., 2009). Once in the air, they are carried upwards by air currents
86 and may remain in the atmosphere for many days before being removed by precipitation or direct
87 deposition onto surfaces. Indeed, the mechanisms that govern the transport, survival, and activity
88 of bacteria in the atmosphere are complex and multifaceted. The interactions between bacteria and
89 their living environment, as well as the atmospheric conditions, play crucial roles in determining
90 their behavior and impacts (Deguillaume et al., 2008).



91 Atmospheric Simulation Chambers (ASCs) have been widely used to study chemical and
92 photochemical atmospheric processes, but the high versatility of these facilities allows for a wider
93 application covering all fields of atmospheric aerosol science. For example, a consistent
94 improvement in characterizing bioaerosols, in understanding the mechanisms affecting their
95 behavior in the atmosphere and finally in elucidating their impacts, can be obtained using
96 atmospheric chamber facilities, where transdisciplinary studies gathering atmospheric physics,
97 chemistry, and biology issues are possible.

98 In the last decades, the use of atmospheric simulation chambers has been much more focused on
99 the potential interest of bioaerosol as ice nuclei and cloud condensation activity (Möhler et al.,
100 2008b; Bundke et al., 2010; Chou, 2011). Recently, addressing the public health concerns related
101 to bioaerosol contamination has led to increased research efforts focusing on the survival and
102 transformation of bioaerosols in the atmospheric environment. Innovative chamber studies have
103 been initiated to investigate these questions and gain insights into the behavior of bioaerosols
104 (Amato et al, 2015; Brotto et al, 2015). These works have led to the development of a new
105 dedicated simulation chamber, ChAMBRe (Massabò et al., 2018). The chamber has been installed
106 at the National Institute of Nuclear Physics in Genoa (IT) in collaboration with the Environmental
107 Physics Laboratory at the Physics Department of the University of Genoa. ChAMBRe is also a
108 National Facility of the constituting ERIC-ACTRIS, the worldwide largest research infrastructure
109 to study atmospheric phenomena, set up by the European Union on April 25th 2023 (CID, 2023).
110 The main scientific target at ChAMBRe, is the description of biological micro-organisms behavior
111 in the atmosphere, aiming to a deeper understanding of the still unclear mechanisms that control
112 the evolution of bioaerosols in atmosphere, in particular their bacterial components. The long-term
113 goal is the parameterization of survival and activity of bioaerosols to develop specific tools to be
114 implemented in chemical transport models (e.g., CAMx, Wagstrom et al., 2008) presently limited
115 to treat transport and chemistry of gaseous and not-biological aerosol species.

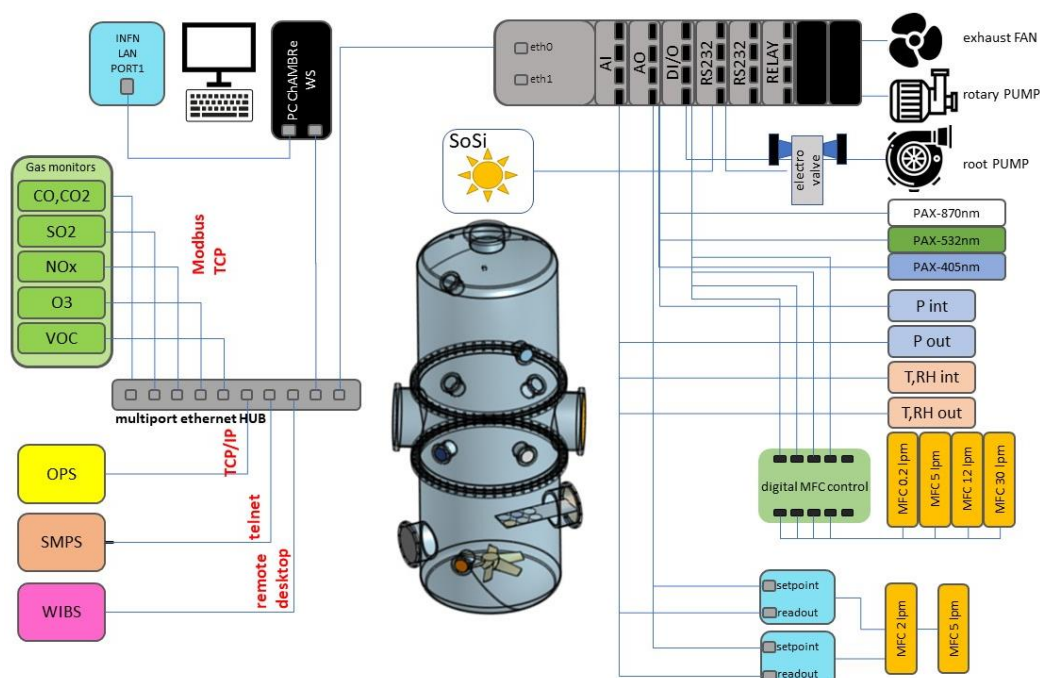
116 This article gives all the details of the present status and capability of the ChAMBRe facility and
117 introduces a multi-step, interdisciplinary procedure assessed to perform quantitative studies on the
118 impact of different pollutants on bacteria viability. Preliminary results are also shown to illustrate
119 the sensitivity of the experimental procedures developed at ChAMBRe that pave the road to
120 systematic investigations on different strains and air quality conditions.

121



122 **2. Material and Methods**

123 Since the beginning of 2017, ChAMBRé has been one of the nodes of the EUROCHAMP-2020
 124 network with specific tasks on bio-aerosol studies. From the date of installation on, ChAMBRé
 125 control and acquisition system has been enriched with a wide range of equipment aimed at
 126 monitoring and controlling the processes occurring inside the chamber. In addition, most efforts
 127 have been devoted to developing protocols to produce, inject, expose and collect bio-aerosols, to
 128 maximize the experiments reproducibility.



129
 130 **Figure 1:** ChAMBRé layout
 131

132 Briefly, ChAMBRé (Massabò et al., 2018) has a cylindrical shape with domed bases. It has a
 133 maximum height and diameter of 2.9 and 1 m, respectively, and a total volume of about 2.2 m³.
 134 The main body is divided into three parts (two domed cylinders connected by a central ring)
 135 equipped with several flanged apertures of different diameters matching the different types of
 136 fitting for instrument interfacing.
 137 To favor the mixing of the gas and aerosol species, a fan is installed at the bottom of the chamber.
 138 It is a standard venting system with a particular pass-through designed and built at INFN-Genoa



139 to ensure the vacuum seal. The fan speed can be regulated by an external controller and set up to
140 50 Hz in steps of 0.1 Hz.

141 One of the two flanges in the bottom part is connected through a pneumatic valve to a smaller
142 horizontal cylinder (length about 1 m), which hosts a movable tray designed to move specific
143 samples inside the chamber. The samples are typically Petri-dishes for bacteria collection inside
144 the chamber during the experiments: they can remain exposed for the whole experiment or for a
145 selected time interval controlled by the user. A custom-made side flange has been worked in the
146 central ring of the main body of the chamber. The large tipper tailgate allows the introduction and
147 positioning of bulky sensor devices for testing and calibration purposes. The flange features a
148 small window for visual inspection and four vacuum feedthrough connectors to power and
149 communicate with devices inserted in the chamber.

150 ChAMBRe is equipped with a composite pumping system (rotary, root and turbo pump) which
151 can evacuate the internal volume to a level of about 5×10^{-4} mbar. The return to atmospheric
152 pressure can proceed by flowing ambient air inside the chamber through a five-stage
153 filtering/purifying/drying inlet system including an absolute HEPA filter and a zeolite trap or using
154 synthetic air from a cylinder (reducing the relative humidity close to zero).

155 Two types of UV lamps are permanently installed inside the chamber. A 58 cm long lamp ($W =$
156 60 W, $\lambda = 253.7$ nm; UV-STYLO-F-60H, Light Progress Srl) is inserted through a custom side
157 flange to sterilize the chamber volume without producing ozone after any experiment involving
158 bioaerosol. A second type of lamp, producing UV radiation at $\lambda < 240$ nm, can be inserted through
159 one of the ISOK100 flanges of the central ring to generate ozone.

160 A set of two pressure gauges is used to measure the atmospheric pressure inside (range 5×10^{-4} -
161 10^3 mbar) and outside (range of 5×10^{-2} - 10^3 mbar). ChAMBRe internal temperature and relative
162 humidity are continuously measured by a sensor located in the upper ISO-K100 flange on the top
163 dome.

164 Supervised injection of known volumes of different gas species inside the chamber is made by a
165 set of software-controlled digital mass flow controllers (MFC) ranging from 5 to 30 lpm full-scale
166 manufactured by Bronkhorst[®]. Two 5-lpm MFCs are dedicated to the injection of CO₂ and SO₂
167 whose concentration inside the chamber can be selected by the operator (ppm or ppb units) and
168 kept constant during the experiment thanks to a PID controller algorithm. A 30-lpm MFC regulates
169 the injection of dry air inside the chamber. In this case the PID controller allows to maintain a pre-



170 defined pressure gap between inside and outside the chamber. A 12-lpm and a 0.2-lpm MFCs are
171 dedicated to the injection of known volumes of air and fuel, respectively, inside the burning
172 chamber of a MISG soot generator device (Argonaut Scientific Corp., Edmonton, 49 AB, Canada,
173 Model MISG–2). The MISG can be connected to an inlet flange of ChAMBR_e for the study of the
174 properties of soot particles exposed and maintained in different conditions or to study the effects
175 of soot particles. The input air flow of the nebulizers, responsible for the crucial process of bacteria
176 injection inside the chamber, is regulated by an analog 5-lpm full-scale MFC (EL-Flow[®])
177 connected to the nebulizer inlet.

178

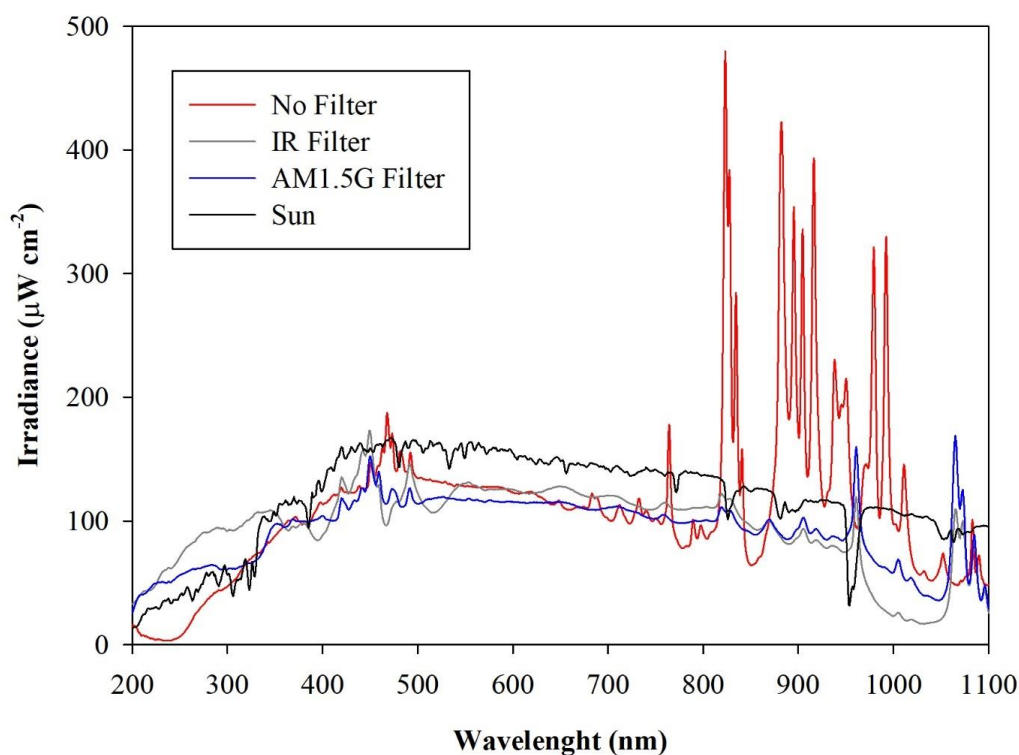
179 *2.1 Instruments permanently connected to the chamber.*

180 The concentration of several gaseous pollutants potentially present inside the chamber (or in the
181 laboratory) can be monitored by a set of calibrated gas detectors manufactured by ENVEA[®]: non-
182 dispersive Carbon monoxide and dioxide analyzer (CO12e), Ozone analyzer (O342e), Sulfur
183 dioxide analyzer (AF22e), chemiluminescent Nitrogen Oxides analyzer (AC32e) and Gas
184 chromatography VOC analyzer (VOC72M). Details on the quoted monitors are provided in
185 Supplement S1.

186 A custom solar simulator manufactured by Sciencetech[™] has been installed on the top of the upper
187 dome of the chamber. The top ISO-K250 flanged aperture has been appropriately modified by
188 inserting a dedicated quartz window (diameter = 25 cm) with a high degree of transmittance (> 95
189 %, with $300 < \lambda < 900$ nm) and reflectance (< 1.5% with $300 < \lambda < 900$ nm) to the solar spectrum
190 radiation. The system consists of two main sections: the light source and the power supply. The
191 light source, a 1600 W Xenon Shor Arc lamp (Sciencetech[™] - XE1600), is mounted inside a
192 dedicated housing where a set of optical lenses and mirrors deflects the light beam perpendicularly
193 to fit the quartz window aperture. A set of filters are available to intercept the light beam and cut-
194 off selectable portions of the spectrum before entering the chamber. In particular, the simulator
195 can be fitted with a low-pass optical filter, designed to cut off a portion of the spectrum in the
196 infrared (IR) region. Alternatively, the optical absorption of the atmosphere can be simulated by
197 using a dedicated filter (AM1.5G 3 × 3" air mass filter, Sciencetech[™]), which cuts off selected
198 bands to mimic the light interaction of an air mass coefficient of 1.5 (i.e., an optical path length
199 that is 1.5 times that of light traversing the atmosphere at the zenith). Figure 1 shows the impact
200 of the available filters on the light spectrum sent to the chamber. The nominal maximum irradiance



201 provided by the Solar Simulator without any filter is about 2.4 SUN, actually 2,424 W m⁻²,
202 corresponding to about 119 W passing through the quartz window on the ChAMBRé top dome
203 with the AM1.5 filter mounted inside the solar simulator.



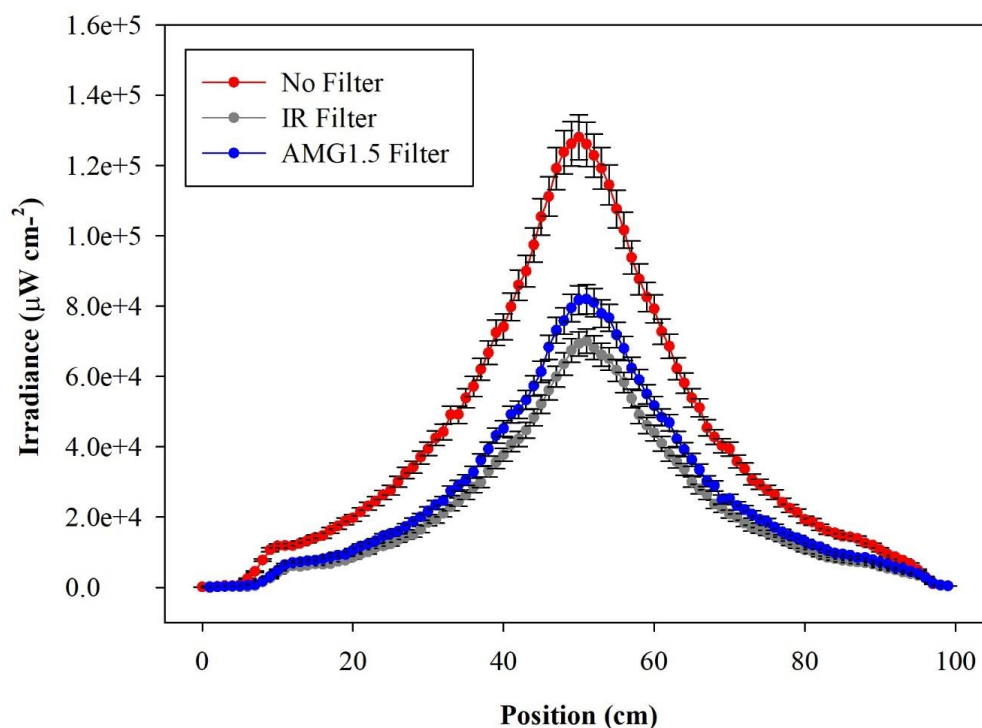
204
205 **Figure 2:** Irradiance vs wavelength measured with a calibrated Avantes ULS2048CL-EVO spectrometer directly at
206 the exit of the Solar Simulator with and without the available filters. The spectrum labelled “Sun” has been
207 measured on a springtime sunny day in the terrace of the Physics Department in Genoa, Italy.

208 The solar simulator is also equipped with a set of four neutral density optical filters, to reduce the
209 light intensity entering the chamber. These filters provide an attenuation of 19%, 34%, 50% and
210 71% of the lamp power, respectively, and can be fitted two at a time on the device, offering a
211 minimum transmittance of 7%. The neutral density filters do not significantly alter the shape of
212 spectrum of the transmitted light, attenuating the optical power uniformly (see Supplement S2,
213 Figure S2).

214 The radial distribution of the optical power measured inside the chamber volume is shown in
215 Figure 3, as a function of the distance along a cross-sectional diameter in the center of ChAMBRé.
216 The light intensity has a strong peak at the center of the diameter, where the optical power is more



217 than six times that close to the walls. To obtain the total light intensity irradiated by the lamp in
218 the chamber volume, the measured data points were fitted with a double gaussian function, which
219 was then integrated in cylindrical coordinates, exploiting the symmetry of the light beam. The
220 resulting intensity is 160 ± 6 W with the lamp set at full power (power supply set at 105% of the
221 nominal value) and no optical filter. The total intensity with the AM1.5 filter is 94 ± 4 W, while
222 with the IR filter the total integrated intensity is 81 ± 4 W. With respect to the irradiance measured
223 directly at the Solar Simulator output, the value inside the chamber shows just a loss of about 20%
224 (likely due focusing/collimation). It must be noted that, at the maximum power and no-filter, the
225 irradiance measured on the middle plane of ChAMBRe is about 0.2 SUN, this almost
226 corresponding to the dilution given by the ratio of the surfaces of the top quartz window (diameter
227 of 25 cm) and of the chamber (diameter of 100 cm).



228

229 **Figure 3:** Irradiance vs wavelength measured with a calibrated Avantes ULS2048CL-EVO spectrometer along a
230 diameter at the center of the ChAMBRe volume, with and without the available optical filters. The center of the
231 chamber is at position=50 cm.



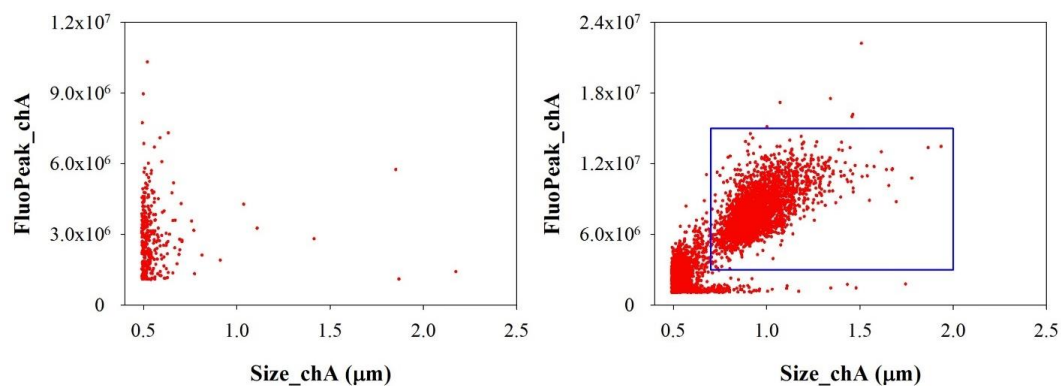
232 Particle concentration and size distribution inside ChAMBRé are real-time monitored by a
233 Scanning Mobility Particle Sizer (SMPS; TSI Inc., model 3938), in the range of 10 – 1000 nm,
234 and an Optical Particle Sizer (OPS; TSI Inc.; model 3330) in the range 0.3 - 10 μm .
235 The SMPS is formed by three components: a neutralizer (i.e., a bipolar diffusion charger), a
236 differential mobility analyzer (DMA, series 3080) and a condensation particle counter (W-CPC,
237 model 3789), from TSI Inc. The model 3088 Neutralizer uses a low-energy ($< 9.5\text{keV}$) soft X-ray
238 source to generate high concentrations of both positive and negative ions to bring the aerosol to a
239 defined, steady-state charge distribution. The DMA is available with two different columns: model
240 3081 Long DMA, which provides the widest size range of 10-1000 nm, and the model 3085 Nano
241 DMA, which covers the range of particle diameter from 2 and 150 nm. In a DMA, an electric field
242 is created and the airborne particles drift in the DMA according to their electrical mobility. Particle
243 size is then calculated from the mobility distribution. In the CPC, downstream of the DMA, the
244 particle size is increased by water condensation on their surface and then the particles are optically
245 counted. The maximum measurable concentration can reach 2×10^5 particles cm^{-3} . The SMPS
246 working airflow ranges between 0.2 and 1.5 lpm.

247 The Model 3330 OPS is an optical particle sizer spectrometer that provides measurement of
248 particle number concentration and particle size distribution based on single particle counting
249 technology. The OPS has an inlet flow rate of $1.0 \text{ lpm} \pm 5\%$ and measures particles from 0.3 μm
250 to 10 μm in 16 user-adjustable size channels (particles above 10 μm are counted but not sized).
251 The OPS 3330 works on the principle of optical scattering from single particles. The OPS uses a
252 laser beam ($\lambda = 660 \text{ nm}$) and a detector to detect particles passing through a sensing volume
253 illuminated by the laser. Particle pulses are counted individually and binned into 16 channels up
254 to their pulse heights. The OPS is factory calibrated using different monodispersed Polystyrene
255 Latex particles (PSL) for size classification; size resolution is 5% at 0.5 μm following the
256 procedure described in the ISO 21501-1 normative. Particles exiting the chamber are trapped by a
257 gravimetric filter for possible after sampling chemical analysis.

258 A Waveband Integrated Bioaerosol Sensor (WIBS-NEO, Droplet Measurement Technologies®)
259 has been integrated in the ChAMBRé particle monitoring system to measure bio-aerosols
260 concentration. The instrument uses two UV filtered flashlamp sources ($\lambda = 280 \text{ nm}$ and $\lambda = 370$
261 nm) to excite fluorescence in individual particles (Lieberherr et al., 2019). Detection wavebands



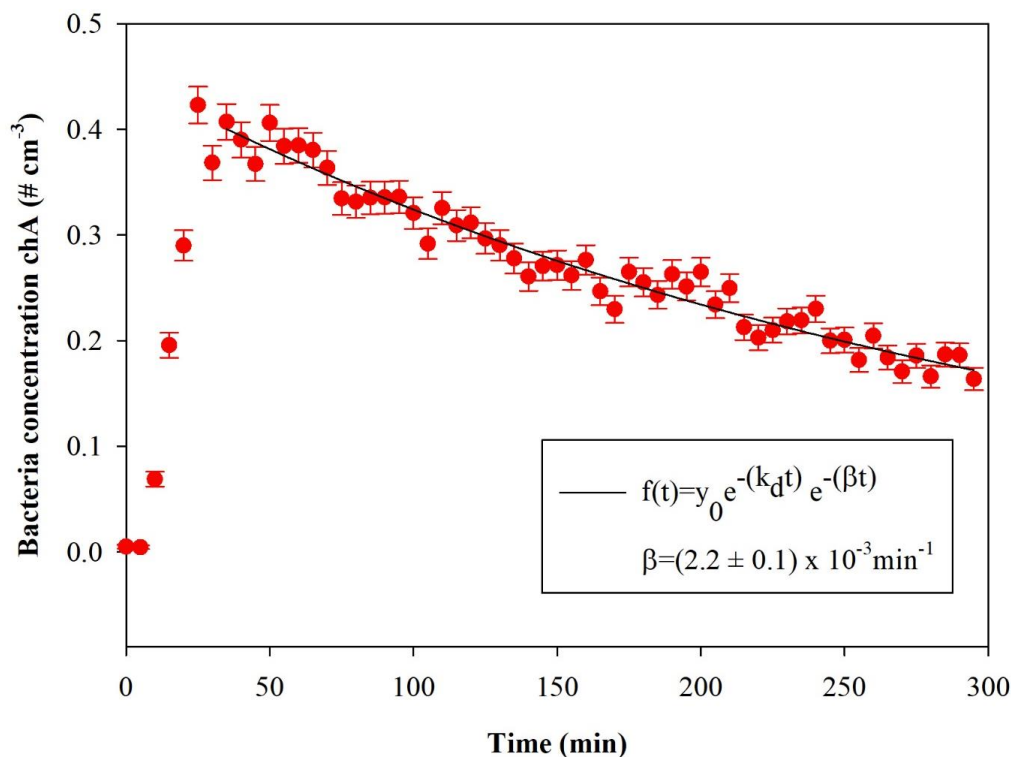
262 have been selected to optimize detection of common bioaerosol components and let the user
263 discriminate between different types of biological micro-organisms (bacteria, fungi, pollen, etc.).
264 The massive amount of data generated by the WIBS during the experiments at ChAMBRe through
265 a list-mode off-line analysis, has made necessary to develop a dedicated software tool, written in
266 Igor 8.0 (Wavemetrics, Inc.) language, aimed at implementing a multi-parametric data reduction
267 and to retrieve the airborne bacteria/bioaerosol concentration inside the chamber as a function of
268 time. Starting from the raw data, the Igor procedure first sets a background threshold for the
269 particle fluorescence intensity and groups the particles into three channels (A, B, C) and their
270 relative intersections (AB, AC, BC, ABC) according to their presence within the three fluorescence
271 detection waveband groups (FL1, FL2, FL3), following the terminology adopted in the WIBS
272 (Lieberherr et al., 2019). Then, for signal-background separation purpose, fiducial cuts are applied
273 on scatter plots (Fluorescence Intensity vs Particle Size) relative to particles belonging to channel
274 A, which is known to be mainly populated by particles showing a bacteria-like fluorescence
275 emission. Examples of the scatter plots are reported in Figure 4 where the region of interest of the
276 signal (*E. coli* bacteria) is well separated from the background region.



277
278 **Fig 4:** Size distribution of particles in channel A. Left: background measured without any bacteria injected in
279 ChAMBRe. Right: particles population after *E. coli* injection. The particles inside the blue rectangular region of
280 interest are identified as *E. coli*.

281

282 Finally, the whole analysis is cycled over user-selectable time intervals to retrieve the time-
283 resolved particle concentration during the whole experiment. Figure 5 shows the time series of *E.*
284 *coli* concentration inside the chamber during a typical experiment.



285

286 **Figure 5:** Temporal trend of *E. coli* particles inside the chamber; $t = 0$ is the injection start. The curve fit is also shown,
 287 where β is the particle loss rate coefficient and k_d is the dilution factor (here $k_d = 1.02 \times 10^{-3} \text{ min}^{-1}$).

288

289 Optical properties (i.e., absorption, extinction and scattering coefficients) of particles suspended
 290 inside the chamber can be measured online by photoacoustic extinction meters (PAXs; Droplet
 291 Measurement Technologies) at three wavelengths: $\lambda = 870, 532$ and 405 nm .
 292 The PAX directly measures in-situ light absorption and scattering of aerosol particles, from which
 293 it derives extinction, single scattering albedo and black carbon mass concentration (Vernocchi et
 294 al., 2022). PAX uses a modulated diode laser to simultaneously measure light scattering and
 295 absorption. The standard infrared, 870 nm wavelength option, is highly specific to black carbon
 296 particles, since there is relatively little absorption from gases and non-BC aerosol species at this
 297 wavelength. A nominal 1 lpm aerosol sample flow is drawn into the PAX using an internal vacuum
 298 pump controlled by two critical orifices. The flow is split between the two distinct measurement
 299 regions: a nephelometer, for the light scattering measurement and a photoacoustic resonator for
 300 the absorption measurement. Absorbing particles heat up and quickly transfer heat to the



301 surrounding air. A sensitive microphone detects the pressure waves produced by the heating,
302 whose intensities are interpreted to infer the particle absorption coefficient (Moosmüller et al.,
303 2009). In the nephelometer, a photodiode set at 90° with respect to the beam detects the radiation
304 reflected by the sampled particles. The scattering measurement responds to all particle types
305 regardless of chemical makeup, mixing state, or morphology.

306 Acquisition and control of the instruments connected to ChAMBRe is handled by a National
307 Instruments™ based system made up of a main controller (NI9057 cRIO) and several modules (C
308 Series modules), which allow communication with the peripheral devices via analog, serial, and
309 ethernet data transfer protocols. The operator interaction with the sensor network is demanded to
310 a single NI-LabVIEW™ SCADA (Supervisory Control And Data Acquisition) custom application
311 which provides the user with a global data overview and a full real-time control above all the
312 instruments parameters via a user-friendly human-machine interface (HMI). In Supplement S1
313 (Figure S1), a screenshot of the main panel of the SCADA application is shown.

314

315 *2.2 Other equipment for specific applications/experiments*

316 Aerosols to be used in ChAMBRe experiments can be generated in different ways, depending on
317 the specific application. The Flow-Focusing Monodisperse Aerosol Generator (FMAG, TSI Inc.
318 model 1520) can be used to produce monodisperse particles in the diameter range 0.8 - 12 µm,
319 starting from both liquid and solid materials. The Mini Inverted Soot Generator (MISG; Argonaut
320 Scientific Corp., model MISG-2) is used to produce soot particles from the controlled combustion
321 of different gaseous fuels (Vernocchi et. al 2022)

322 Three nebulizers, designed for bioaerosol applications, are also available: the Collison nebulizer,
323 the Blaustein Atomizing Modules (BLAM), and the Sparging Liquid Aerosol Generator (SLAG),
324 all manufactured and distributed by CH TECHNOLOGIES Inc. The performances of the three
325 nebulizers in connection to the injection of viable bacteria in the chamber have been previously
326 investigated and described in (Danelli et al., 2021).

327 Bacteria injected inside ChAMBRe can be collected by different methods. A cylindrical horizontal
328 volume is connected to the chamber by an ISO-KF250 pneumatic valve; this volume can be
329 alternatively opened or closed without perturbing the inner atmosphere thanks to another ISO-
330 KF250 pneumatic valve. Inside the cylinder, there is a sliding tray that can be inserted in
331 ChAMBRe by an external manual control, to minimize the risk of contamination. The tray can



332 host up to six Petri dishes (diameter 10 cm, each) to collect bacteria (or in general BPA) directly
333 by gravitational settling. In addition, bacteria can be collected on solid medium (i.e., Petri dishes
334 filled with culture medium) by the active sampling by an Andersen impactor (Single Stage
335 Andersen Cascade Impactor, TISCH Environmental) working at a fixed air flow of 28.3 lpm,
336 supplied by a dedicated pump. The impactor is connected to the chamber by ISO-K flanges.
337 Moreover, bioaerosol can be collected through liquid impinger, (Flow Impinger, Aquaria srl),
338 filled with 20 ml of sterile liquid solution, allowing subsequent offline laboratory analysis. Such a
339 device can be easily connected to the chamber volume through the ISO-K flanges. Impinger
340 operates at a constant airflow of 12.5 lpm (e.g., by a low-capacity pump: Model LCP5, Copley
341 Scientific). Finally, aerosol suspended in the chamber can be also collected on filters (i.e., quartz
342 fibre, PTFE, cellulose) for offline analysis. Sampling is managed by a low-volume particulate
343 matter sampler, setting the air flow in the range 10 – 50 lpm.

344

345 *2.3. Equipment to manipulate bioaerosol*

346 A biological laboratory with specific instrumentation for isolating and maintaining bacterial cells
347 culture is part of the ChAMBRé facility:

- 348 • Biosafety cabinet, and laminar flow hood, Miniflow Linear blue air Aquaria, (Milano,
349 Italy). It is used to provide a contamination-free working environment for the workers. A
350 laminar flow filters the air and traps dust particles and microbes for providing a sterile
351 working environment in the stainless-steel cabinet. The hood is equipped with HEPA filter
352 and UV-light laminar is created inside the cabinet.
- 353 • Centrifuge MPW-352 MPW MED Instruments (Warsaw, Poland) used to separate particles
354 from a homogeneous solution through rotational movement and centrifugal acceleration,
355 causing sedimentation of its components. The MPW-352 has a swinging-bucket rotor that
356 swings out when centripetal force is applied and holds the pellet at an approximate 90°
357 angle relative to the angle of rotation.
- 358 • Spectrophotometer Shimadzu 1900 is a double-beam UV-Vis Shimadzu Corporation,
359 Japan. This instrument measures intensity as a function of light source wavelength. For
360 each wavelength of light passing through the spectrometer, the intensity of the light passing
361 through the sample cell is measured. The biological applications include measurement of



362 substance concentration such as protein, DNA or RNA, growth of bacterial cells, and
363 enzymatic reactions.

- 364 • Shaker incubator with orbital rotation movement SKI 4 ARGOLAB, Carpi MO – Italy. It
365 provides a controlled environment for samples to grow and develop while also providing
366 mechanical agitation to mimic the natural movement of cells in their environment. Shaking
367 can be used to promote the growth and development of cells and microorganisms to
368 increase the oxygen supply to the cells. The oxygen is an important factor that can affect
369 the growth and metabolism of cells. By shaking the culture, it is possible to increase the
370 oxygen supply to the cells by increasing the diffusion of oxygen into the media.
- 371 • Quantum Tx microbial cell counter Logos Biosystems, South Korea. This automated cell
372 counter can detect individual bacterial cells in a liquid sample. The instrument provides
373 counting of the total number of cells in the suspension using fluorescent probe. It captures
374 images of (10-fields) fluorescence-stained cells and automatically it counts the bacterial
375 cells. The optimal concentration range of count is $5 \times 10^5 - 5 \times 10^8$ cells ml⁻¹ and the size
376 range of the count cells is between 0.3 and 50 μm . The sample is prepared from the bacterial
377 suspension in physiological solution immediately before injection; for counting the total
378 number of cells, three different solutions to 10 μl of the initial suspension are added: *Total*
379 *Cell Staining Dye*, *Total Cell Staining Enhancer* and *Loading Buffer I*. The first added is
380 the *Total Cell Staining Dye*, a membrane-permeable fluorescent dye, which is capable of
381 binding to nucleic acids in viable and non-viable cells and allows the detection of Gram-
382 positive and Gram-negative bacteria. This probe has an excitation wavelength of $\lambda = 484$
383 nm, and it emits $\lambda = 504$ nm. The second solution used is the *Total Cell Staining Enhancer*
384 to guarantee a better cells penetration by the probe and to obtain a uniform background
385 during the images acquisition by Quantum Tx. The sample must be incubated in the dark
386 at 37°C for about 30 minutes to favor the penetration of the fluorescent dye into the cells.
387 Finally, the *Loading Buffer I* is added and used to uniform the distribution and the
388 sedimentation of bacterial cells in the counting stands. The slide, after being centrifuged at
389 300 RCF for 10 minutes, is inserted in the specific support in the counter and then
390 illuminated with a lamp at $\lambda = 470$ nm with a bandpass of 30 nm. The light power can be
391 set to nine levels of intensity (labelled from 1 to 9): in our experiments, the best results are
392 obtained selecting the intensity of 5 for counting total cells.



393 *2.3.1 Bacteria cultivation, injection and monitoring*

394 The bacteria strain so far used to perform experiments at ChAMBRé is *Escherichia coli* (ATCC®
395 25922™), Gram-negative, purchased by Thermo Scientific™ Culti-Loops™. *E. coli* is rod-shaped,
396 about 1–2 µm long and about 0.25 µm in diameter (Jang et al., 2017). It is a common inhabitant of
397 the gastrointestinal apparatus of warm-blooded animals, including humans. This strain is a non-
398 pathogen proxies of typical atmospheric bacteria, extensively used as model organisms in
399 microbiology and molecular biology fundamental and applied studies (Lee et al., 2002; Lee and
400 Kim, 2003).

401 Bacterial growth is a complex process that involves several distinct phases. The increase in
402 numbers or bacterial mass can be measured as a function of time under culture conditions where
403 the nutrients and environmental conditions are controlled. Several distinct growth phases can be
404 observed within a growth curve such as the lag phase, the exponential or log phase, the stationary
405 phase, and the death phase. The first stage, the lag phase, occurs when bacteria are not dividing
406 but are metabolically active. During the lag phase of the bacterial growth cycle, the synthesis of
407 RNA, enzymes, and other molecules occurs. The length of this phase depends on the type of
408 bacterial species, culture medium, and environmental factors. The log phase is an exponential
409 phase characterized by rapid growth, with binary fission. The number of new bacteria appearing
410 per unit time is proportional to the present population. If growth is not limited, doubling will
411 continue at a constant rate, so both the number of cells and the rate of population increase doubles
412 with each consecutive period. Exponential growth cannot continue indefinitely, however, because
413 the medium is soon depleted of nutrients and enriched with catabolites. (Maier R. et al., 2008).
414 The stationary phase is due to a growth-limiting factor; this is mostly depletion of a nutrient, and/or
415 the formation of inhibitory products such as organic acids. Instead during the death phase, the
416 number of living cells decreases exponentially. Bacteria run out of nutrients and die although the
417 number of cells stays constant. The decline phase is brought by exhaustion of nutrients,
418 accumulation of toxic products, and autolytic enzymes. The microbial growth curve is a record of
419 the countable cells determined at certain time intervals during the population's evolution. In our
420 work, the calibration curve was figured out converting the rate growth from OD values to CFU
421 (Colony Forming Unit) ml⁻¹, as explained in detail below.



422 The day before the experiment, bacteria cells are scraped off agar medium, where they are
423 cultivated, using sterile plastic loops and suspended in a sterile, non-selective culture broth
424 medium Tryptic Soy Broth (TSB) and incubated overnight at 37 °C. The day after, 3 ml of the
425 bacteria culture is diluted in 30 ml of new broth medium, and the suspension is incubated again at
426 37 °C. At intervals of about thirty minutes, the OD of the bacterial solution is measured by the
427 spectrophotometer at $\lambda = 600$ nm; OD_{600nm} allows to estimate the concentration of bacterial cells
428 in the liquid and tracking the growth. The mid-exponential phase is typically reached when
429 OD_{600nm} is about 0.5 (Mytilinaios et al., 2012; Hall et al., 2014). For selected OD values, the
430 bacterial concentration was also measured/referred as Colony Forming Units (CFU). The bacteria
431 solution must be diluted several times to obtain not overlapping colonies on Petri Dishes: 100 μ l
432 of bacterial solution is added in 900 μ l of sterile saline solution (NaCl 0.9 %), then diluted again
433 as many times as the theoretical concentration (calculated using the OD value) required; 100 μ l of
434 the last dilution is spread in duplicate on an TSB agar and incubated overnight at 37 °C. The next
435 day the concentration of culturable cells is measured by counting the colonies formed and
436 multiplying by the proper dilution factor to retrieve CFU concentration in the original solution.
437 Data, obtained by CFU counting on agar plates, are averaged and used to figure out the uncertainty
438 of the bacterial concentration in the solution following the Poisson statistics.
439 Several sigmoidal functions were so far adopted to describe a bacterial growth curve. The literature
440 on these models is well known and is used in various contests: plants, bird growth, fish and other
441 animals, cancers and bacterial growth (Kathleen M. et al., 2017). We tested the fits to our *E. coli*
442 growth curves by Logistic, Gompertz, and Richards models. (Birch C.P. 1999; Baty F. and
443 Delignette-Muller M.L. 2004). The logistic function model is used specifically to describe growth
444 of microorganisms, as a function of nutrient depletion (Daniel E. W. et al 2003) and it was
445 demonstrated to be the best fit for modeling bacteria (Akin et al 2020; Annadurai G. et al. 2000).
446 Here, the results of the logistic fit are only shown. The logistic equation was written as:

447

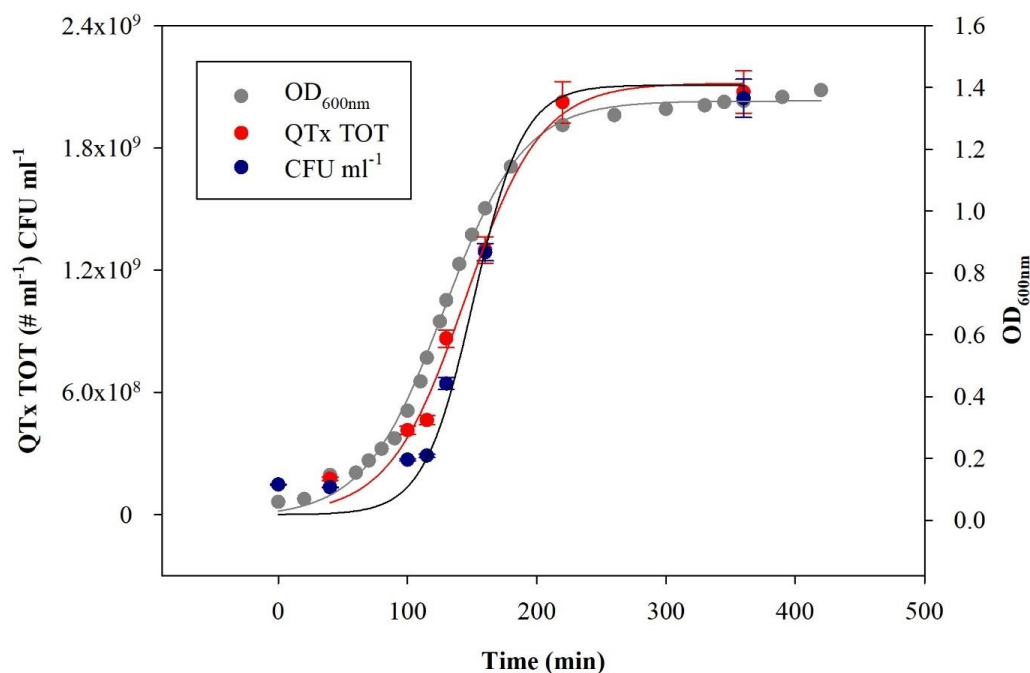
$$448 \quad y(t) = \frac{y_0}{1 + e^{-b(t-t_0)}} \quad (1)$$

449

450 where y indicates the bacteria concentration in the solution, y_0 is the saturation value, b is the
451 maximum specific growth rate and t_0 is the time at the inflection point.



452 We followed the growth of *E. coli* in suspension culture for about 8 hours from lag phase to
 453 horizontal asymptote and the OD_{600nm}, the total number of *E. coli* (QTx TOT), measured with
 454 Quantum TX and the CFU ml⁻¹ values are reported in Figure 6. The values of reduced chi-squared,
 455 (χ^2), y_0 , b and t_0 of the logistic fit for OD_{600nm}, QTx TOT and CFU ml⁻¹ are reported in Table 1.



456
 457 **Figure 6:** Grow curve for *E. coli*: optical density (OD_{600nm}), total number of *E. coli* measured by QUANTOM-TX (#
 458 ml⁻¹) and the corresponding bacteria concentration (CFU ml⁻¹) vs. time. Error bars are, in most cases, the same size
 459 as the data points.
 460

461 **Table 1:** χ^2 , y_0 , b and t_0 of the logistic fit for OD_{600nm}, QTx TOT and CFU ml⁻¹.

Logistic 3 parameters	OD _{600nm}	QTx TOT (# ml ⁻¹)	CFU ml ⁻¹
χ^2	1.04	1.17	1.17
y_0	1.35 ± 0.01	$(212 \pm 8) \times 10^7$	$(211 \pm 6) \times 10^7$
b (min ⁻¹)	$(3.3 \pm 0.1) \times 10^{-2}$	$(3.4 \pm 0.5) \times 10^{-2}$	$(5.2 \pm 0.4) \times 10^{-2}$
t_0 (min)	128 ± 1	145 ± 5	151 ± 2

462
 463 OD_{600nm} and QTx TOT have the same value of the b parameter and this result is expected since the
 464 OD_{600nm} is an indirect measurement of the total concentration of cells in suspension. The grow rate



465 of CFU ml⁻¹ is faster and the corresponding doubling time (about 19 minutes) is compatible with
466 the value reported in the literature (Son M.S. et al, 2001).

467

468 2.3.2 Bacteria and experiments in ChAMBR_e

469 To prepare the inoculum for the chamber experiments, the *E. coli* is grown in fresh TSB
470 nonselective medium, in a shaking incubator at 37 °C and 200 rpm and its growth is followed by
471 checking the OD_{600nm} value until the mid-exponential phase. When OD_{600nm} ~ 0.5, the bacteria are
472 centrifugated at 3000 rpm for 10 min. Afterward, bacteria are resuspended in a sterile physiological
473 solution (NaCl 0.9 % w/v) and the number of cultivable cells is counted as CFU by standard
474 dilution plating on Petri dishes filled with TSB and Agar. Plated Petri dishes are then incubated at
475 37 °C for 24 h before counting. Four Petri dishes, with two different dilution levels, are prepared,
476 and then the number of the counted colonies are averaged, to retrieve the bacterial concentration
477 in the solution and its statistical uncertainty. The dilution levels for plating were 10^{-4.5} and 10⁻⁵:
478 these serial dilutions were selected to obtain a number of CFUs in the range 20-150.

479 For the experiments performed at ChAMBR_e, the typical bacterial concentration in the inoculum
480 is 10⁷ CFU ml⁻¹: to reach this concentration, a further dilution step is needed (i.e., typically 1:10
481 or 1:5) before the injection.

482 The concentration of the solution to be injected inside ChAMBR_e is also controlled in terms of
483 total cells ml⁻¹ by Quantom Tx Microbial Cell Counter. The sample is prepared from the bacterial
484 suspension in physiological solution. In each single analysis, Quantom Tx acquires 10 visual fields
485 of the slide's counting chamber, which correspond to an approx. volume of 0.09 µl, to retrieve the
486 bacterial count. To evaluate if the exposure of Quantom Tx lamp degrades the fluorescent probe
487 (photobleaching) of total cells, we repeated the total cell counts inserting and ejecting 10 times the
488 same sample: the total count probe didn't show a particular sensitivity to the exposure to the
489 Quantom Tx lamp, and the relative standard deviation turned out to be less than 5%. Further details
490 on the use of Quantom Tx counter are given in Supplement S4.

491 The bacteria suspension, properly diluted, is injected into the chamber volume mainly by using the
492 Sparging Liquid Aerosol Generator, SLAG, which ensured the better reproducibility in earlier tests
493 (Danelli et al., 2021). The injection phase typically lasts 5 minutes. Injection air flow and duration
494 are automatically controlled by a Mass Flow Controller (Bronkhorst, model F201C-FA) managed
495 via SCADA. In this way, 2 ml of bacterial suspension are nebulized inside ChAMBR_e.



496 Experiments with *E. coli* were performed by active sampling via the Andersen impactor: sampling
497 time was progressively increased after the injection to collect a suitable number of CFUs. At time
498 $t = 0$ (three minutes after the conclusion of the injection to allow proper mixing/homogenization
499 inside the ChAMBRé volume), three petri were consecutively sampled. The variability on the
500 CFUs collected on the three petri, calculated as the ratio between standard deviation and mean
501 value, resulted equal to 12%. Sampling time during *E. coli* experiments are summarized in Table
502 S2 in Supplement S5.

503 After the experiments in the simulation chamber, the plates sampled are incubated at 37 °C for 24
504 h. The CFUs are then counted and, in the experiments conducted by active sampling, the CFU cm⁻³
505 are calculated.

506 The possible correlation between bacteria viability and air quality can be investigated in terms of
507 change in bacteria viability due to the exposure to atmospheric pollutants. Effects on bacteria
508 viability are compared in relation to “baseline experiments”. In a baseline experiment, the viability
509 of airborne bacteria is measured at atmospheric pressure, with temperatures around 20°C and with
510 relative humidity around 60%: such values have been chosen to reproduce an environment suitable
511 for the survival of bacteria (Dunklin E.W. 1948; Cox C.S. 1966; Benbough J.E. 1967). During
512 baseline experiments, the bacteria's viability depended on their characteristics and experimental
513 procedures only. The baseline was assessed both in “dark” and “light” conditions. With “light”
514 condition, the Solar Simulator was used with the AM1.5 filter mounted (see 2.1) to reduce the UV
515 radiation; several experiments were replicated with the Solar Simulator lamp intensity set at 105%
516 and 80% of the nominal value (i.e., the maximum and minimum intensity level which guarantees
517 stability without using neutral filters). Baseline experiments, see Section 3, were particularly
518 important also to assess the reproducibility and hence the sensitivity of the whole procedure.

519 The baseline assessment was followed by a set of exploratory experiments with *E. coli* exposed to
520 selected pollutants. We measured the possible bacterial viability changes due to the exposure to
521 atmospheric conditions typically met in polluted urban areas. So far, *E. coli* was exposed to
522 different concentrations of NO and NO₂, two of the most common pollutants emitted by vehicular
523 and ship traffics (Seinfeld and Pandis, 1998; Monks et al., 2009; Pöschl and Shiraiwa, 2015;).

524



525 **3. Results**

526 The experiments performed to investigate the possible effects on bacteria viability due to the
527 exposure to atmospheric pollutants, were conducted by following the same procedure adopted to
528 assess the baseline and introducing inside ChAMBRé the specific pollutant. During gas pollutant
529 experiments, NO or NO₂ concentration was kept constant thanks to the feedback control system
530 described in 2.1.3.

531

532 *3.1 Baseline experiments with E. coli in dark conditions.*

533 *E. coli* behavior in a set of baseline experiments was first determined in dark conditions. The
534 average total concentration of *E. coli* inside the chamber immediately after the injection was (0.34
535 ± 0.03) cells cm⁻³, measured by the WIBS; the average viable concentration, determined by the
536 Andersen impactor sampling just after the injection (i.e., after 3 minutes of mixing time), was (0.04
537 ± 0.01) cells cm⁻³. The average ratio of viable:total (V:T in the following) bacteria concentration
538 inside ChAMBRé, at the beginning of the experiments therefore turned out to be V:T = (0.13 ±
539 0.03) with the viable cells counted in terms of CFUs. The total and viable bacteria concentration
540 values measured inside ChAMBRé depended on the V:T ratio in the inoculum to be injected and
541 on the aerosolization process affecting the bacteria viability. However, it is worthy to note the
542 stability of baseline results despite the variability of the V:T ratio measured in the bacteria
543 inoculum before the injection (see figure 7 and 8). The bacteria viable concentration was
544 determined via standard dilution plating while the bacteria total concentration was calculated by
545 the Quantom Tx. During baseline experiments, the V:T ratio of the inoculum ranged between 0.25
546 ± 0.03 and 0.50 ± 0.06. Time-trends of total and viable concentration of the bacteria nebulize inside
547 ChAMBRé are shown in Figure 6. Average values are the result of eight replicated experiments.
548 Bacteria lifetime in ChAMBRé can be calculated by fitting the data with an exponential function
549 as:

550

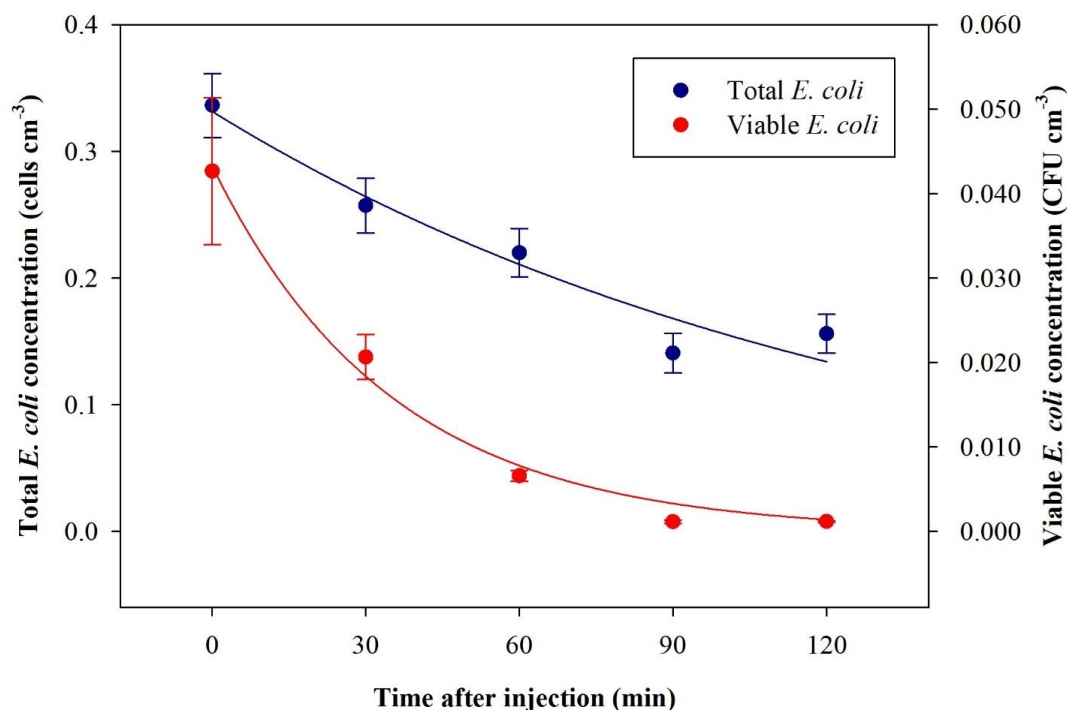
551

$$C(t) = C_0 e^{-\frac{t}{\tau}} \quad (2)$$

552



553 where C_0 is the average of total or viable concentration of *E. coli* just after the injection and τ is
 554 the total or viable bacteria lifetime, respectively. In table 2, C_0 and τ for the total and viable
 555 concentration of *E. coli* are reported.



556

557 **Figure 7:** Time-trend of *E. coli* average bacteria total (red) and viable (green) concentration inside ChAMBRé
 558 obtained by eight repetitions of baseline experiments.

559

560 **Table 2:** C_0 and τ of the exponential fit for total and viable concentration of *E. coli*.

Exponential function	Total <i>E. coli</i>	Viable <i>E. coli</i>
C_0	(0.33 ± 0.02) cells cm ⁻³	(0.043 ± 0.002) CFU cm ⁻³
τ (min)	125 ± 16	34 ± 4

561

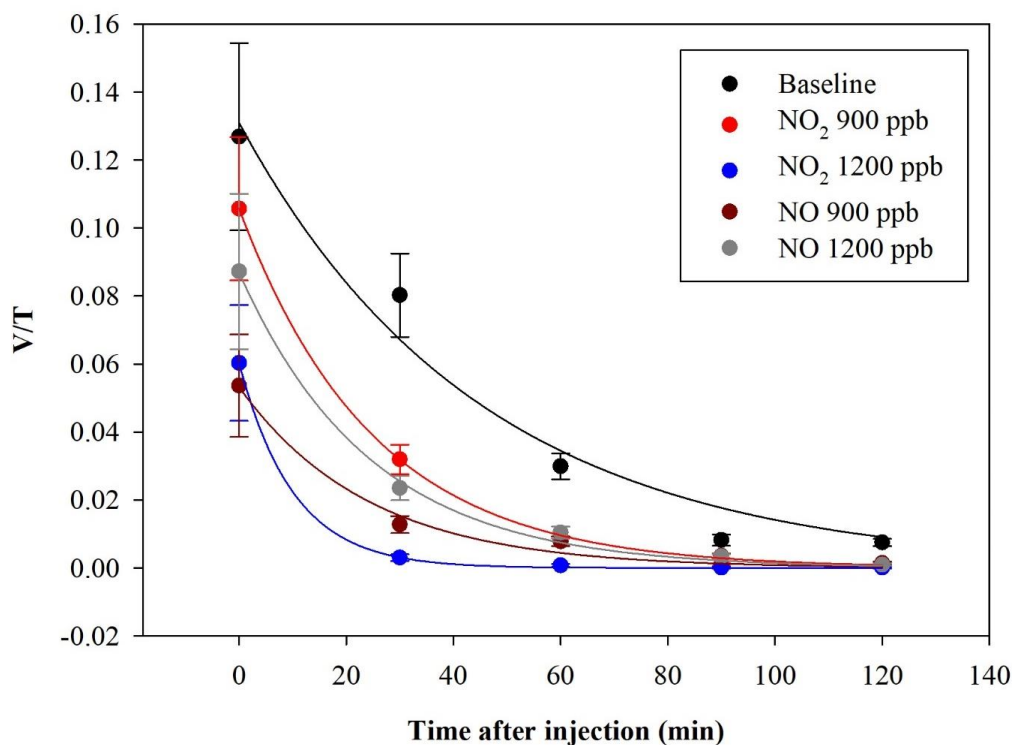
562 The total *E. coli* lifetime is about 125 minutes; this value agrees with data reported in (Massabò et
 563 al., 2018) for generic aerosols: particles, in the size range of 1 – 2 μm ($\tau = 2\text{--}3$ hours), the same of
 564 *E. coli*. The viable *E. coli* lifetime is about 34 minutes, lower than the aerodynamic lifetime, this
 565 indicating the difficulty of this microorganism to survive in the atmospheric medium.



566 3.2 Experiments with *E. coli* and NO_x in dark conditions.

567 A preliminary check was performed exposing the *E. coli* to O₃, which is recognized to be a strong
568 antimicrobial agent (Kim et al., 1999; Giuliani et al., 2018; Thanomsub et al., 2022), hence the
569 expected result was a complete viability loss. The exposure of bacteria to O₃ (concentration > 1000
570 ppb) resulted in a roughly complete cell mortality, as expected. The initial condition immediately
571 after the injection was V:T = (0.03 ± 0.01) and no CFUs were collected in any of the following
572 samplings (starting 30 minutes after the injection).

573 Then, bacteria were exposed to NO₂ and NO concentrations, 900 and 1200 ppb for both the
574 pollutants. The exposure of bacteria to such pollutants showed a V:T reduction. The average
575 results, obtained in a set of eight experiments, are shown in Figure 8.



576

577 **Figure 8:** Time-trend of the V:T ratio for *E. coli* in baseline (black) and in the experiments with ChAMBRe maintained
578 at a constant concentration of: NO₂ (900 ppb red and 1200 ppb blue) and NO (900 ppb dark red and 1200 ppb gray).



579 The quantitative reduction in the *E. coli* lifetime, due to the exposure to pollutants, can be evaluated
580 considering the V:T ratio and fitting the data with an exponential curve, as previously described;
581 the results are shown in Table 3.

582 **Table 3:** Initial values and τ of the exponential fit for V:T ratio of *E. coli* at different pollutants concentrations.

Exponential function	(V:T t=0)	τ (min)
Baseline	0.13 ± 0.01	45 ± 6
NO ₂ 900 ppb	0.106 ± 0.001	25 ± 1
NO ₂ 1200 ppb	0.0603 ± 0.0003	10.1 ± 0.4
NO 900 ppb	0.053 ± 0.003	24 ± 3
NO 1200 ppb	0.087 ± 0.002	24 ± 2

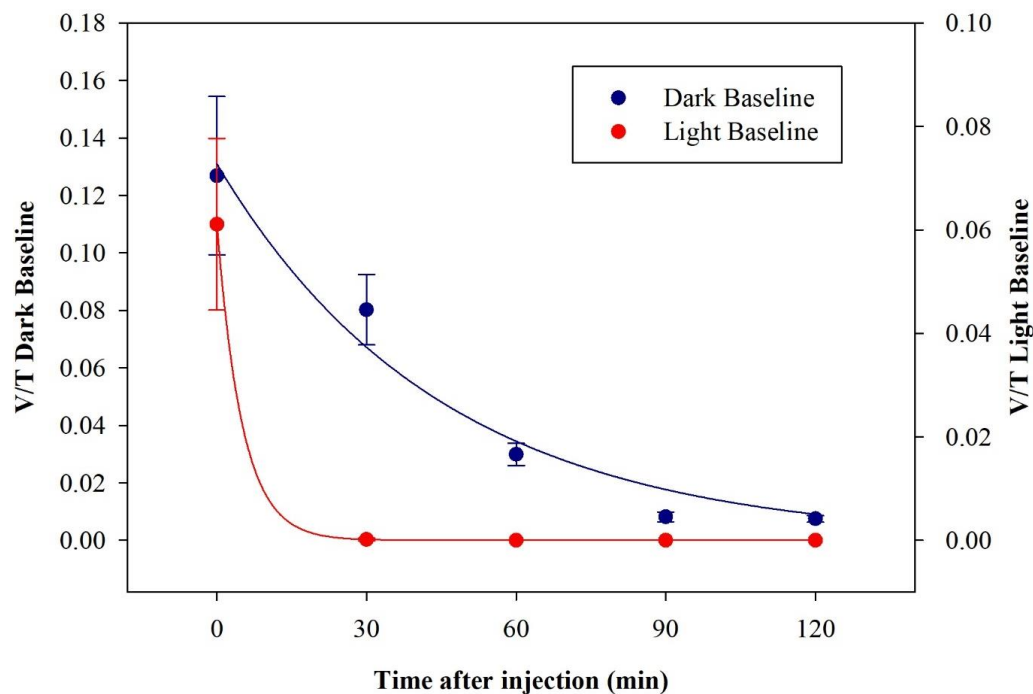
583

584 *E. coli* lifetime in baseline experiments, calculated on the V:T ratio, turned out to be about 45 min.
585 The exposure of *E. coli* to NO₂ reduced the lifetime to about 25 and 10 min with a concentration
586 of 900 ppb and 1200 ppb respectively. The exposure to NO decreased bacteria lifetime to 24 min
587 for both concentrations and they are equal to the value obtained with the lowest NO₂ concentration;
588 this suggests that NO₂ is more toxic for *E. coli* than NO. In addition, the increase of the NO
589 concentration did not correspond to a decrease in the *E. coli* viability, as observed with NO₂.

590

591 3.2 Experiments with *E. coli* and Solar Simulator.

592 *E. coli* behavior when exposed to light was determined in a set of dedicated baseline experiments.
593 No significant differences in results appeared changing the intensity of the Solar Simulator
594 operated with the AM1.5G filter and data are here gathered. After the injection, the average total
595 concentration of *E. coli* reached inside the chamber was (0.30 ± 0.03) cells cm⁻³, compatible with
596 the dark baseline; while the average viable concentration was (0.019 ± 0.005) cells cm⁻³, lower
597 than what obtained in dark experiments. The consequent V:T ratio was (0.06 ± 0.02) . The viable
598 concentration collapses after 30 minutes, V:T = $(4.7 \pm 7.1) 10^{-5}$ cells cm⁻³ and reaches zero after
599 an hour. The comparison between V:T ratio obtained for dark and light baseline is shown in Figure
600 8.



601

602 **Figure 9:** Time-trend of the V:T ratio for *E. coli* in the dark baseline (dark blue) and light baseline (red) experiments.

603

604 These results indicate a significant decrease in bacteria viability due to their exposure to solar
605 radiation. The behavior, here evaluated in atmospheric environment, agrees with observation in
606 water environments reported in several works (Whitman et al., 2004; Jozić et al., 2014; Tiwari et
607 al., 2022); the solar radiation is indicated as an abiotic factor with the negative effect of bringing
608 some bacteria strains, among which *E. coli*, into a temporary inactivation/non-cultivable state.

609

610 **4. Discussion, conclusion and perspectives**

611 The main result presented in this work is the assessment of a multi-step and well controlled
612 protocol to perform experiments on the impact of air quality on bacteria viability by an atmospheric
613 simulation chamber, ChAMBRe in this case. Even if the chamber configuration is still in progress
614 and several new equipment will be deployed at ChAMBRe in the next future, the present set-up
615 opens the possibility of systematic studies. The reproducibility of the baseline reference, based on
616 the active bacteria sampling by a one-stage Andersen impactor, turned out to be at the 20% level
617 and this corresponds to the experimental sensitivity for changes in the *E. coli* viability due to



618 exposure to pollutants and/or other relevant parameters. The baseline reference must be
619 experimentally determined for each bacteria strain and efforts are planned for repeating the
620 observation with *Bacillus subtilis*, *Bacillus spizizenii* and *Pseudomonas fluorescens* in the next
621 future. It is worthy to note that the experimental protocol returns the lifetime of total and viable
622 bacteria injected in the chamber. The figure for total bacteria corresponds to the aerodynamic
623 behavior of aerosol of diameter around 1 μm , already reported in (Massabò et al., 2008) while the
624 lifetime of viable bacteria is much shorter (about half an hour) due to the difficulty of this
625 microorganism to survive in the atmospheric medium. Such shorter lifetime posed clear constraints
626 on the first experiments with exposure of *E. coli* to NO_x inside ChAMBRe. A time window of two
627 hours after the bacteria injection was considered to observe the behavior of *E. coli* viability and it
628 was possible to quantify a lifetime reduction, in dark conditions, clearly related to NO and NO_2
629 concentration inside ChAMBRe. These findings pave the road to systematic studies including
630 other bacteria strains and pollutant species. With the *E. coli* exposed to the light produced by the
631 Solar Simulator operated with the AM1.5 filter, the viability resulted very short even in the
632 baseline conditions and therefore no further experiment with pollutants was performed. With other
633 bacterial strains, the impact of light on viability will have to be reinvestigated.

634

635 **5. Acknowledgments**

636 We are indebted to the personnel of the mechanical workshop of the INFN division of Genoa for
637 the continuous support in the development of the ChAMBRe structure. The development of the
638 chamber and the deployment of the equipment was supported by several European and Italian
639 projects/grants: EUROCHAMP2020 (H2020: Infrastructure Activity under grant agreement No
640 730997); PON per-ACTRIS-IT (MUR-IT: PON project PIR_00015 “Per ACTRIS IT”); BLUE-
641 LAB NET (F.E.S.R. - FONDO EUROPEO DI SVILUPPO REGIONALE Azione POR, Regione
642 Liguria, IT); ATMO-ACCESS (H2020: Infrastructure Activity under grant agreement No
643 101008004); NextGenerationEU PNRR-ITINERIS (Italian Integrated Environmental Research
644 Infrastructures System).

645

646

647



648 **6. References**

- 649 Akin, E., Pelen, N. N., Tiryaki, I. U., Yalcin, F.: Parameter identification for Gompertz and logistic
650 dynamic equations, *PLoS ONE* 15(4): e0230582, <https://doi.org/10.1371/journal.pone.0230582>,
651 2020.
- 652 Amato, P., Ménager, M., Sancelme, M., Laj, P., Mailhot, G., Delort, A. -M.: Microbial population
653 in cloud water at the Puy de Dôme: Implications for the chemistry of clouds, *Atmos. Environ.* 39,
654 4143–4153, <https://doi.org/10.1016/j.atmosenv.2005.04.002>, 2005.
- 655 Amato, P., Parazols, M., Sancelme, M., Laj, P., Mailhot, G., Delort, A. -M. : Microorganisms
656 isolated from the water phase of tropospheric clouds at the Puy de Dôme : major groups and growth
657 abilities at low temperatures, *FEMS Microbiol. Ecol.* 59, 242–254, [https://doi.org/10.1111/j.1574-](https://doi.org/10.1111/j.1574-6941.2006.00199.x)
658 6941.2006.00199.x, 2006.
- 659 Amato, P., Demeer, F., Melaouhi, A., Fontanella, S., Martin-Biesse, A.-S., Sancelme, M., Laj, P.,
660 Delort, A.-M.: A fate for organic acids, formaldehyde and methanol in cloud water: their
661 biotransformation by micro-organisms, *Atmospheric Chem. Phys.* 7, 4159–4169,
662 <https://doi.org/10.5194/acp-7-4159-2007>, 2007.
- 663 Amato, P., Joly, M., Schaupp, C., Attard, E., Möhler, O., Morris, C.E., Brunet, Y., Delort, A.-M.:
664 Survival and ice nucleation activity of bacteria as aerosols in a cloud simulation chamber,
665 *Atmospheric Chem. Phys.* 15, 6455–6465. <https://doi.org/10.5194/acp-15-6455-2015>, 2015.
- 666 Annadurai, G., Rajesh Babu, S., Srinivasamoorthy, V. R.: Development of mathematical models
667 (Logistic, Gompertz and Richards models) describing the growth pattern of *Pseudomonas putida*
668 (NICM 2174), *Bioprocess Engineering*, 23(6), 607-612, <https://doi.org/10.1007/s004490000209>,
669 2000.
- 670 Ariya, P.A., Nepotchatykh, O., Ignatova, O., Amyot, M. : Microbiological degradation of
671 atmospheric organic compounds, *Geophysical Research Letters* 29, NO. 22, 2077,
672 <https://doi.org/10.1029/2002GL015637>, 2002.
- 673 Ariya, P.A., Amyot, M.: New Directions: The role of bioaerosols in atmospheric chemistry and
674 physics, *Atmos. Environ.* 38, 1231–1232, <https://doi.org/10.1016/j.atmosenv.2003.12.006>, 2004.
- 675 Baty, F., Delignette-Muller, M. L. : Estimating the bacterial lag time : which model, which
676 precision?, *International journal of food microbiology*, 91(3), 261-277,
677 <https://doi.org/10.1016/j.ijfoodmicro.2003.07.002>, 2004.
- 678 Bauer, H., Kasper-Giebl, A., Zibuschka, F., Hitzenberger, R., Kraus, G. F., Puxbaum, H.:
679 Determination of the Carbon Content of Airborne Fungal Spores, *Anal. Chem.*, 74, 1, 91–95,
680 <https://doi.org/10.1021/ac010331+>, 2002.
- 681 Benbough, J. E.: Death Mechanisms in Airborne *Escherichia coli*, *J. Gen. Microbiol.* 47, 325–
682 333, <https://doi.org/10.1099/00221287-47-3-325>, 1967.



- 683 Birch, C. P. D.: A new generalized logistic sigmoid growth equation compared with the Richards
684 growth equation, *Annals of botany*, 83(6), 713-723, <https://doi.org/10.1006/anbo.1999.0877>,
685 1999.
- 686 Brotto, P., Repetto, B., Formenti, P., Pangui, E., Livet, A., Bousserhine, N., Martini, I., Varnier,
687 O., Doussin, J.F., Prati, P.: Use of an atmospheric simulation chamber for bioaerosol investigation:
688 a feasibility study, *Aerobiologia* 31, 445–455, <https://doi.org/10.1007/s10453-015-9378-2>, 2015.
- 689 Bowers, R. M., McLetchie, S., Knight, R., Fierer, N.: Spatial variability in airborne bacterial
690 communities across land-use types and their relationship to the bacterial communities of potential
691 source environments. *ISME J.* 5, 601–612, <https://doi.org/10.1038/ismej.2010.167>, 2011.
- 692 Bundke, U., Reimann, B., Nillius, B., Jaenicke, R., Bingemer, H.: Development of a Bioaerosol
693 single particle detector (BIO IN) for the Fast Ice Nucleus Chamber FINCH, *Atmos. Meas. Tech.*,
694 3, 263–271, <https://doi.org/10.5194/amt-3-263-2010>, 2010.
- 695 Burrows, S. M., Butler, T., Jöckel, P., Tost, H., Kerkweg, A., Pöschl, U., Lawrence, M.G.: Bacteria
696 in the global atmosphere – Part 2: Modeling of emissions and transport between different
697 ecosystems, *Atmospheric Chem. Phys.* 9, 9281–9297. <https://doi.org/10.5194/acp-9-9281-2009>,
698 2009.
- 699 Chou, C., Stetzer, O., Weingartner, E., Jurányi, Z., Kanji, Z. A., Lohmann, U.: Ice nuclei properties
700 within a Saharan dust event at the Jungfraujoch in the Swiss Alps, *Atmos. Chem. Phys.*, 11, 4725–
701 4738, <https://doi.org/10.5194/acp-11-4725-2011>, 2011.
- 702 CID, Commission Implementing Decision (EU) 2023/900, “Setting up the Aerosol, Clouds and
703 Trace Gases Research Infrastructure (ACTRIS ERIC)” Official Journal of the European Union
704 L115/15, 03/05/2023.
- 705 Cox, C.S.: The Survival of *Escherichia coli* sprayed into Air and into Nitrogen from Distilled
706 Water and from Solutions of Protecting Agents, as a Function of Relative Humidity, *J. Gen.*
707 *Microbiol.* 43, 383–399, <https://doi.org/10.1099/00221287-43-3-383>, 1966.
- 708 Danelli, S., Brunoldi, M., Massabò, D., Parodi, F., Vernocchi, V., Prati, P.: Comparative
709 characterization of the performance of bio-aerosol nebulizers in connection with atmospheric
710 simulation chambers. *Atmos. Meas. Tech.*, 14, 4461–4470, [https://doi.org/10.5194/amt-14-4461-](https://doi.org/10.5194/amt-14-4461-2021)
711 2021, 2021.
- 712 Deguillaume, L., Leriche, M., Amato, P., Ariya, P.A., Delort, A.-M., Pöschl, U., Chaumerliac, N.,
713 Bauer, H., Flossmann, A.I., Morris, C.E.: Microbiology and atmospheric processes: chemical
714 interactions of primary biological aerosols, *Biogeosciences* 5, 1073–1084,
715 <https://doi.org/10.5194/bg-5-1073-2008>, 2008.
- 716 Després, V. R., Huffman, J. A., Burrows, S. M., Hoose, C., Safatov, A. S., Buryak, G., Fröhlich-
717 Nowoisky, J., Elbert, W., Andreae, M.O., Pöschl, U., Jaenicke, R.: Primary biological aerosol
718 particles in the atmosphere: a review. *Tellus B Chem. Phys. Meteorol.* 64, 15598,
719 <https://doi.org/10.3402/tellusb.v64i0.15598>, 2012.



- 720 Dunklin, E. W., Puck, T. T.: The lethal effect of relative humidity on airborne bacteria. *J. Exp.*
721 *Med.* 87, 87–101, <https://doi.org/10.1084/jem.87.2.87>, 1948.
- 722 Fröhlich-Nowoisky, J., Kampf, C. J., Weber, B., Huffman, J. A., Pöhlker, C., Andreae, M. O.,
723 Lang-Yona, N., Burrows, S. M., Gunthe, S. S., Elbert, W., Su, H., Hoor, P., Thines, E., Hoffmann,
724 T., Després, V. R., Pöschl, U.: Bioaerosols in the Earth system: Climate, health, and ecosystem
725 interactions. *Atmospheric Res.* 182, 346–376, <https://doi.org/10.1016/j.atmosres.2016.07.018>,
726 2016.
- 727 Giuliani, G., Ricevuti, G., Galoforo, A., Franzini, M.: Microbiological aspects of ozone:
728 bactericidal activity and antibiotic/antimicrobial resistance in bacterial strains treated with ozone.
729 *Ozone Therapy*, 3(3), <https://doi.org/10.4081/ozone.2018.7971>, 2018.
- 730 Griffin, D., Westphal, D., Gray, M.: Airborne microorganisms in the African desert dust corridor
731 over the mid-Atlantic ridge, Ocean Drilling Program, Leg 209, *Aerobiologia* 22, 211–226,
732 <https://doi.org/10.1007/s10453-006-9033-z>, 2006.
- 733 Hall, B. G., Acar, H., Nandipati, A., Barlow, M.: Growth Rates Made Easy, *Mol. Biol. Evol.* 31,
734 232–238, <https://doi.org/10.1093/molbev/mst187>, 2014.
- 735 Jang, J., Hur, H.-G., Sadowsky, M. J., Byappanahalli, M. N., Yan, T., Ishii, S.: Environmental
736 *Escherichia coli*: ecology and public health implications-a review, *J. Appl. Microbiol.* 123, 570–
737 581, <https://doi.org/10.1111/jam.13468>, 2017.
- 738 Jozić, S., Morović, M., Šolić, M., Krstulović, N., Ordulj, M.: Effect of solar radiation, temperature
739 and salinity on the survival of two different strains of *Escherichia coli*, *Fresenius Environ. Bull.*
740 23, 1852–1859, 2014.
- 741 Tjørve, K. M. C., Tjørve, E.: The use of Gompertz models in growth analyses, and new Gompertz-
742 model approach: An addition to the Unified-Richards family, *PLOS ONE* June 5, 2017,
743 <https://doi.org/10.1371/journal.pone.0178691>, 2017.
- 744 Kim, J. G., Yousef, A. E., Dave, S.: Application of Ozone for Enhancing the Microbiological
745 Safety and Quality of Foods: A Review, *Journal of Food Protection*, 62, 9, 1071-1087,
746 <https://doi.org/10.4315/0362-028X-62.9.1071>, 1999.
- 747 Kolbe, U., Yi, B., Poth, T., Saunders, A., Boutin, S., Dalpke, A. H.: Early Cytokine Induction
748 Upon *Pseudomonas aeruginosa* Infection in Murine Precision Cut Lung Slices Depends on Sensing
749 of Bacterial Viability, *Frontiers in Immunology* 2020, 11:598636,
750 <https://doi.org/10.3389/fimmu.2020.598636>, 2020.
- 751 Lee, B. U., Kim, S. H., Kim, S. S.: Hygroscopic growth of *E. coli* and *B. subtilis* bioaerosols,
752 *Journal of Aerosol Science* 33, 1721–1723, [https://doi.org/10.1016/S0021-8502\(02\)00114-3](https://doi.org/10.1016/S0021-8502(02)00114-3),
753 2002.
- 754 Lee, B. U., Kim, S. S.: Sampling *E. coli* and *B. subtilis* bacteria bioaerosols by a new type of
755 impactor with a cooled impaction plate, *J. Aerosol Sci.*, 34, 1097–1100, 2003.



- 756 Lieberherr, G., Auderset, K., Calpini, B., Clot, B., Crouzy, B., Gysel-Beer, M., Konzelmann, T.,
757 Manzano, J., Mihajlovic, A., Moallemi, A., O'Connor, D., Sikoparija, B., Sauvageat, E., Tummon,
758 F., Vasilatou, K.: Assessment of real-time bioaerosol particle counters using reference chamber
759 experiments, *Atmos. Meas. Tech.*, 14, 7693–7706, <https://doi.org/10.5194/amt-14-7693-2021>,
760 2021.
- 761 Lighthart, B.: The ecology of bacteria in the alfresco atmosphere, *FEMS Microbiol. Ecol.* 23, 263–
762 274, <https://doi.org/10.1111/j.1574-6941.1997.tb00408.x>, 2006.
- 763 Mainelis, G., Berry, D., Reoun An, H., Yao, M., DeVoe, K., Fennell, D.E., Jaeger, R.: Design and
764 performance of a single-pass bubbling bioaerosol generator, *Atmos. Environ.* 39, 3521– 3533,
765 <https://doi.org/10.1016/j.atmosenv.2005.02.043>, 2005.
- 766 Martiny, J. B. H., Bohannan, B. J. M., Brown, J. H., Colwell, R. K., Fuhrman, J. A., Green, J. L.,
767 Horner-Devine, M. C., Kane, M., Krumins, J. A., Kuske, C. R., Morin, P. J., Naeem, S., Ovreås,
768 L., Reysenbach, A.-L., Smith, V. H., Staley, J. T.: Microbial biogeography: putting
769 microorganisms on the map. *Nat. Rev. Microbiol.* 4, 102–112,
770 <https://doi.org/10.1038/nrmicro1341>, 2006.
- 771 Massabò, D., Danelli, S. G., Brotto, P., Comite, A., Costa, C., Di Cesare, A., Doussin, J. F.,
772 Ferraro, F., Formenti, P., Gatta, E., Negretti, L., Oliva, M., Parodi, F., Vezzulli, L., Prati, P.:
773 ChAMBRé: a new atmospheric simulation chamber for aerosol modelling and bio-aerosol
774 research, *Atmos. Meas. Tech.*, 11, 5885–5900, <https://doi.org/10.5194/amt-11-5885-2018>, 2018.
- 775 Möhler, O., DeMott, P. J., Vali, G., Levin, Z.: Microbiology and atmospheric processes: the role
776 of biological particles in cloud physics, *Biogeosciences* 4, 1059–1071, <https://doi.org/10.5194/bg-4-1059-2007>, 2007.
- 778 Monks, P. S., Granier, C., Fuzzi, S., Stohl, A., Williams, M. L., Akimoto, H., Amann, M.,
779 Baklanov, A., Baltensperger, U., Bey, I., Blake, N., Blake, R. S., Carslaw, K., Cooper, O. R.,
780 Dentener, F., Fowler, D., Fragkou, E., Frost, G. J., Generoso, S., Ginoux, P., Grewe, V., Guenther,
781 A., Hansson, H. C., Henne, S., Hjorth, J., Hofzumahaus, A., Huntrieser, H., Isaksen, I. S. A.,
782 Jenkin, M. E., Kaiser, J., Kanakidou, M., Klimont, Z., Kulmala, M., Laj, P., Lawrence, M. G., Lee,
783 J. D., Liousse, C., Maione, M., McFiggans, G., Metzger, A., Mieville, A., Moussiopoulos, N.,
784 Orlando, J. J., O'Dowd, C. D., Palmer, P. I., Parrish, D. D., Petzold, A., Platt, U., Pöschl, U.,
785 Prévôt, A. S. H., Reeves, C. E., Reimann, S., Rudich, Y., Sellegri, K., Steinbrecher, R., Simpson,
786 D., ten Brink, H., Theloke, J., van der Werf, G. R., Vautard, R., Vestreng, V., Vlachokostas, Ch.,
787 von Glasow, R.: Atmospheric composition change – global and regional air quality, *Atmos.*
788 *Environ.* 43, 5268–5350, <https://doi.org/10.1016/j.atmosenv.2009.08.021>, 2009.
- 789 Morris, C. E., Georgakopoulos, D. G., Sands, D. C.: Ice nucleation active bacteria and their
790 potential role in precipitation. *J. Phys. IV Proc.* 121, 87–103,
791 <https://doi.org/10.1051/jp4:2004121004>, 2004.
- 792 Morris, C. E., Leyronas, C., Nicot, P. C.: Movement of Bioaerosols in the Atmosphere and the
793 Consequences for Climate and Microbial Evolution, in: Colbeck, I., Lazaridis, M. (Eds.), *Aerosol*



- 794 Science: Technology and Applications. John Wiley & Sons, Ltd, Chichester, UK, pp. 393–415,
795 <https://doi.org/10.1002/9781118682555.ch16>, 2014.
- 796 Mytilinaios, I., Salih, M., Schofield, H. K., Lambert, R. J. W.: Growth curve prediction from
797 optical density data, *Int. J. Food Microbiol.* 154, 169–176,
798 <https://doi.org/10.1016/j.ijfoodmicro.2011.12.035>, 2012.
- 799 Pöschl, U.: Atmospheric Aerosols: Composition, Transformation, Climate and Health Effects,
800 *Angew. Chem. Int. Ed.* 44, 7520–7540, <https://doi.org/10.1002/anie.200501122>, 2005.
- 801 Pöschl, U., Shiraiwa, M.: Multiphase Chemistry at the Atmosphere–Biosphere Interface
802 Influencing Climate and Public Health in the Anthropocene, *Chem. Rev.* 115, 4440–4475,
803 <https://doi.org/10.1021/cr500487s>, 2015.
- 804 Prospero, J., Blades, E., Mathison, G., Naidu, R. : Interhemispheric transport of viable fungi and
805 bacteria from Africa to the Caribbean with soil dust, *Aerobiologia* 21, 1–19,
806 <https://doi.org/10.1007/s10453-004-5872-7>, 2005.
- 807 Romano, S., Di Salvo, M., Rispoli, G., Alifano, P., Perrone, M. R., Talà, A.: Airborne bacteria in
808 the Central Mediterranean: Structure and role of meteorology and air mass transport, *Science of
809 the Total Environment* 697 (2019) 134020, <https://doi.org/10.1016/j.scitotenv.2020.138899>, 2019.
- 810 Seinfeld, J. H., Pandis, S. N.: 1998. Atmospheric Chemistry and Physics: From Air Pollution to
811 Climate Change, Wiley-Interscience, ISBN 10: 0471178152 ISBN 13: 9780471178156, 1997.
- 812 Shaffer, B.T., Lighthart, B.: Survey of Culturable Airborne Bacteria at Four Diverse Locations in
813 Oregon: Urban, Rural, Forest, and Coastal, *Microb. Ecol.* 34, 167–177,
814 <https://doi.org/10.1007/s002489900046>, 1997.
- 815 Son, M. S., Taylor R. K.: Growth and Maintenance of *Escherichia coli* Laboratory Strains, *Curr.
816 Protoc.* 2021 January; 1(1): e20, <https://doi.org/10.1002/cpz1.20>, 2021.
- 817 Sun, J., Ariya, P.: Atmospheric organic and bio-aerosols as cloud condensation nuclei (CCN): A
818 review, *Atmos. Environ.* 40, 795–820, <https://doi.org/10.1016/j.atmosenv.2005.05.052>, 2006.
- 819 Thanomsub, B., Anupunpisit, V., Chanphetch, S., Watcharachaipong, T., Poonkhum, R., and
820 Srisukonth, C.: Effects of ozone treatment on cell growth and ultrastructural changes in bacteria,
821 *J. Gen. Appl. Microbiol.*, 48, 193–199, <https://doi.org/10.2323/jgam.48.193>, 2002.
- 822 Tiwari, A., Kauppinen, A., Räsänen, P., Salonen, J., Wessels, L., Juntunen, J., Miettinen, I. T.,
823 Pitkänen, T.: Effects of temperature and light exposure on the decay characteristics of fecal
824 indicators, norovirus, and Legionella in mesocosms simulating subarctic river water, *Sci. Tot. Env.*
825 859, <https://doi.org/10.1016/j.scitotenv.2022.160340>, 2022.
- 826 Tong, Y., Lighthart, B.: Diurnal Distribution of Total and Culturable Atmospheric Bacteria at a
827 Rural Site. *Aerosol Sci. Technol.* 30, 246–254, <https://doi.org/10.1080/027868299304822>, 1999.



- 828 Vernocchi, V., Brunoldi, M., Danelli, S. G., Parodi, F., Prati, P., Massabò, D.: Characterization of
829 soot produced by the mini-inverted soot generator with an atmospheric simulation chamber,
830 *Atmos. Meas. Tech.*, 15, 2159–2175, <https://doi.org/10.5194/amt-15-2159-2022>, 2022.
- 831 Wagstrom, K. M., Pandis, S. N., Yarwood, G., Wilson, G. M., Morris, R. E.: Development and
832 application of a computationally efficient particulate matter apportionment algorithm in a three-
833 dimensional chemical transport model. *Atmos. Environ.* 42 (2008) 5650–5659,
834 <https://doi.org/10.1016/j.atmosenv.2008.03.012>, 2008.
- 835 Wang, C.-C., Fang, G.-C., Lee, L.: Bioaerosols study in central Taiwan during summer season,
836 *Toxicol. Ind. Health* 23, 133–139, <https://doi.org/10.1177/0748233707078741>, 2007.
- 837 Whitman, R. L., Nevers, M. B., Korinek, G.C., Byappanahalli, M.N.: Solar and temporal effects
838 on *Escherichia coli* concentration at a Lake Michigan swimming beach, *Appl Environ Microbiol.*
839 Vol 70, No. 7, <https://doi.org/10.1128/AEM.70.7.4276-4285.2004>, 2004.
- 840 Zwietering, M. H., Jongenburger, I., Rombouts, F. M., van 't Riet, K.: Modeling of the bacterial
841 growth curve, *Appl Environ Microbiol.* 1990 Jun; 56(6): 1875–1881, DOI:
842 <https://doi.org/10.1128/aem.56.6.1875-1881.1990>, 1990.